ZnO Nanostructures Doped with Various Chloride Ion Concentrations for Efficient Photocatalytic Degradation of Methylene Blue in Alkaline and Acidic Media

Razan A Alshgari, Zaheer Ahmed Ujjan, Aqeel Ahmed Shah, Muhammad Ali Bhatti, Aneela Tahira, Nek Muhammad Shaikh, Susheel Kumar, Mazhar Hussain Ibupoto, Amal Elhawary, Ayman Nafady, et al.

ZnO nanostructures doped with various chloride ion concentrations for efficient photocatalytic degradation of methylene blue in alkaline and acidic media

Razan A. Alshgari[a], Zaheer Ahmed Ujjan[b], Aqeel Ahmed Shah[d], Muhammad Ali Bhatti[c], Aneela Tahira[b], Nek Muhammad Shaikh[b], Susheel Kumar[a], Mazhar Hussain Ibupoto[eh], Amal Elhawary[f] Ayman Nafady[a], Brigitte Vigolo[g], Zafar Hussain Ibupoto[b]

[a]Department of Chemistry, College of Science, King Saud University, Riyadh 11451, Saudi Arabia

[b]Institute of Physics University of Sindh Jamshoro, 76080, Sindh Pakistan

[c]Dr. M.A Kazi Institute of Chemistry University of Sindh Jamshoro, 76080, Sindh Pakistan

[d]Institute of Environmental Sciences, University of Sindh Jamshoro, 76080, Sindh Pakistan

[e]NED University of engineering and Technology Karachi, Pakistan

[f] Department of Chemistry and physics, Faculty of Education, Alexandria University, Alexandria, Egypt

[g]Université de Lorraine, CNRS, IJL, F-54000 Nancy, France

[g]Department of Zoology, Shah Abdul Latif University Khairpur Mirs

***Corresponding authors** : Zafar HussainIbupoto, PD.PD.PhD, Zaheer Ahmed Ujjan, PhD

Email: zaffar.ibhupoto@usindh.edu.pk, ujjanzaheer@gmail.com

Abstract

In this study, chloride (Cl^-) ion is successfully doped into ZnO nanostructures by wet chemical method. The effect of Cl^- concentration on the photocatalytic activity of ZnO towards the degradation of methylene blue (MB) is studied. The as-prepared Cl^--doped ZnO nanostructures were analysed in terms of morphology, structure, composition and optical properties. XRD data has revealed an average crystallite size of 10 nm and the XRD patterns were assigned to wurtzite structure of ZnO even after doping with Cl^-. Importantly, the optical band gap of ZnO was reduced from 3.42 to 3.12 eV upon increasing the concentration of Cl^- dopant. The photodegradation efficiency of various Cl^--doped ZnO nanostructures for MB was probed and followed the order (20 % Cl^--doped ZnO > 15% Cl^--doped ZnO > 10%

Cl^--doped ZnO > 5%Cl^-doped ZnO > pristine ZnO). Furthermore, the effect of pH on the degradation rate of MB using Cl^--doped ZnO was also explored . The combined results clearly attest on the crucial role of Cl^- ions in activating the degradation kinetics of MB when doped into ZnO photocatalyst compare to pristine counterpart. Therefore, these newly developed photocatalysts could be considered for important practical applications such as wastewater treatment.

Keywords: Chloride (Cl^-) concentration, ZnO, Methylene blue, Photodegradation

1 Introduction

Various strategies have been employed to expel natural organic dyes such as leather products, pharmaceuticals, printing, food industries, modern coatings, and plastics from contaminated water [1-5]. In view of the high molecular weight and synthetic steadiness of organic dyes, conventional methods such as physio-compounds and biochemicals normally don't offer complete degradation of environmental contaminants [6]. Therefore, searching for new approaches for removal of harmful dyes such as methylene blue (MB) from wastewater becomes highly demand to maintain the aquatic life and environment. In recent years, a number of heterogeneous photosensitive materials have been applied for the photodegradation and wastewater treatment, [7] owing to marked advantages such as low cost, efficiency and stability under normal atmospheric conditions [8-10]. In this respect, zinc oxide (ZnO) is a semiconductor photocatalyst in group II-VI, which possesses a large energy band gap of 3.37 (eV) and high exciton energy (60 m eV), respectively along with being highly thermally and mechanically stable at room temperature [11-14]. Given the large band gap of ZnO, it requires large photonic energy for the photoexcitation process. Hence, photocatalytic activity can’t take place in some of the charge carriers due to loss of energy during recombination of electron-hole pairs. The pristine ZnO has a fast recombination of photogenerated electron-hole pairs, thereby resulting in deterioration of the photocatalytic properties.

The prevention of fast recombination rate with effective charge transport and separating efficiency of charge carriers could be achieved by introducing dopant as an electron scavenger, thus enabling the material to increase the period of electrons in excited state and also absorption spectrum broadness could also be increased [15-17]. In view of these findings, the doping process is anticipated to contribute in three ways: (1) reducing band gap energy and enhancing

adsorption, (2) decreasing resistivity and promoting mobility of charge carriers, and (3) varying the position of conduction and valence band. In this context, ZnO as a semiconducting material has been doped with other elements to reduce the fast recombination process and efficiently separate out the photogenerated electrons and holes [18, 19]. Among approaches for ZnO doping, sol-gel [20-22], hydrothermal [23-25] and chemical vapour deposition [26, 27], semiconductor coupling [28, 29] surface hybridization of ZnO with carbon [30], and combustion [31-35] have been implemented. Literature survey reveals that doping of ZnO with non-metals such as carbon(C), nitrogen (N), and sulphurs (S) tunes the intermediate energy level band gap as well as tuning the ability to absorb visible light which leads to enhanced photocatalytic activity [36-40]. Moreover, the Cl^- doped ZnO nanostructures have been reported for optical applications [41-44]. However, to the best of our knowledge, the effect of Cl^- ion concentration on the optical properties of ZnO towards the degradation of MB has not been reported, particularly under the acidic and basic conditions.

In this contribution, we describe a facile procedure for doping various concentrations of Cl^- ions into ZnO nanostructures using wet chemical method. Additionally, the effect of various Cl^- -doped ZnO on driving the degradation kinetics of MB is studied under different pH value. The synthesized 20% Cl^- -doped ZnO showed remarkable photocatalytic efficiency for degradation of MB at pH 11.

2 Materials and methods

2.1 Used chemicals

Zinc acetate-dihydrate ($ZnC_4H_6O_4$), 25% aqueous ammonia solution Merck), methylene blue ($C_{16}H_{18}ClN_3S$) organic dye, and ethanol (C_2H_5OH, 99.5%) were provided by Sigma-Aldrich Karachi Pakistan and used without further purification. The methylene blue was dissolved in the deionized water and material synthesis was also performed in the deionized water. The chemical structure of methylene Blue (MB) is shown in Figure. 1.

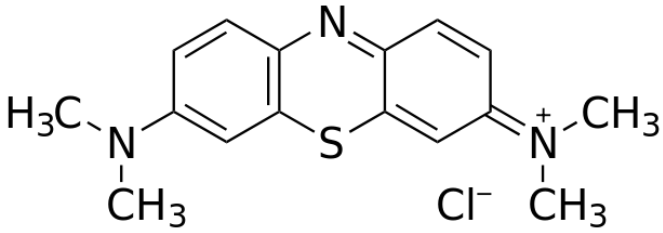

Figure 1 shows structure of methylene blue

2.2 Preparation of various Cl^- -doped ZnO nanostructures by wet chemical method

The preparation of pristine ZnO and Cl^--doped ZnO was performed via using of wet chemical method by mixing zinc acetate di-hydrate ($ZnC_4H_6O_4$) and 25% ammonia as precursors for the fabrication of ZnO. The different concentration of ammonium chloride (% w.w) such as 5, 10, 15 and 20% were mixed in 5 mL of ethanol in four beakers and an ultrasonic bath was employed for 30 min to obtain well dispersion. Then, 2.22 g of zinc acetate di-hydrate was dissolved by slowly adding 5mL of 25% ammonia solution. Four of them with sole concentration of ammonium chloride ranging from 5, 10, 15 and 20 % mixed with (5 mL) of ethanol solution thereby labeling applied as a 5% Cl^--doped ZnO, 10% Cl^--doped ZnO, 15% Cl^--doped ZnO, and 20% Cl^--doped ZnO to identify the different samples. To avoid the evaporation of aqueous solution the beakers were sealed with aluminum foil. The nanostructure of the Cl^--doped ZnO were grown in a muffle furnace at 90°C for 5 hrs. Finally, the four synthesized Cl^--doped ZnO nanostructured samples were collected via filtration and drying process. The pristine ZnO material was obtained by same process without the use of Cl^- source.

2.3 The evaluation of photodegradation effectiveness of various Cl^--doped ZnO nanostructures

The effect of pH values on the phototocatalytic activity of the as-synthesized pristine ZnO and Cl^--doped ZnO was examined in aqueous media. Typically, the reaction suspension was prepared using 10 mg of Cl^--doped ZnO powder into 100 mL of 0.0001M. The aqueous suspension of nanostructures was placed in sonication bath for 30 min which resulted in adsorption-desorption equilibrium. The UV-Visible light irradiation was carried out in a locally made photoreactor using a compact UV lamp of (365 nm) and a power of 18 watt. The UV–Visible spectrophotometer (PE Lamda35) was employed to quantify absorbance peak of MB dye, which was detected at (664) nm. After every 15 min of UV-Vis irradiation, the amount of MB was monitored by sampling out 5mL of aqueous solution. The degradation of MB observed in intensity in absorption characteristic wavelength of (664) nm by recording UV-Vis spectra in the wavelength range of 200 – 800 nm. The mathematical formula for the evaluation of degradation activity of pristine ZnO and Cl^--doped ZnO samples was as follows

$$Degradation\ Efficiency\ (\%) = \left(\frac{A_o - A}{A_o}\right) \times 100 \quad (1)$$

Where A_o is absorbance of fresh dye solution without photo treatment (mg/L), A represents the absorbance of MB dye (mg/L) at various irradiating times of UV light.

3. Results and discussion

3.1 Crystalline, morphology and composition studied of Cl^-doped ZnO nanostructures

Figure. 2(a) depicts the powder X-ray diffraction patterns of pristine ZnO and Cl^- -doped ZnO nanostructures over the range of 23^o to 78^o. The various reflection peak positions and intensities of Cl^- -doped ZnO were measured at 2Θ angle such as 31.86° (100), 34.54° (002), 36.32° (101), 47.62° (102), 56.66° (110), 62.96° (103), 66.44° (200), 68.04° (112), 69.18° (201), which are fully supported by the JCPDS card No. 01-075-1533. A wurtzite phase of ZnO was confirmed. No additional peaks corresponding to group 17 elements (Halogens) and its oxide phase was obtained, thereby confirming that all samples were in crystalline nature and wurtzite structure [45]. This could be attributed to substitution of Zn ions by Cl^- ions from the lattice without letting the disturbance in the hexagonal structure of ZnO. However, an increasing order in the red shift in peak position plane (102) at the angle of (47.476°) in both pristine ZnO and Cl^- -doped ZnO samples was observed, which might alter the optical properties due to the difference in the size of Cl^- and Zn atoms, as shown in Figure 2(b). Furthermore, the obtained values of lattice parameters a and c and volumes of pure and Cl^- -doped ZnO nanostructures were observed in increasing order, suggesting the incorporation of Cl^- atom into ZnO as shown in Figure 2 (c-e).

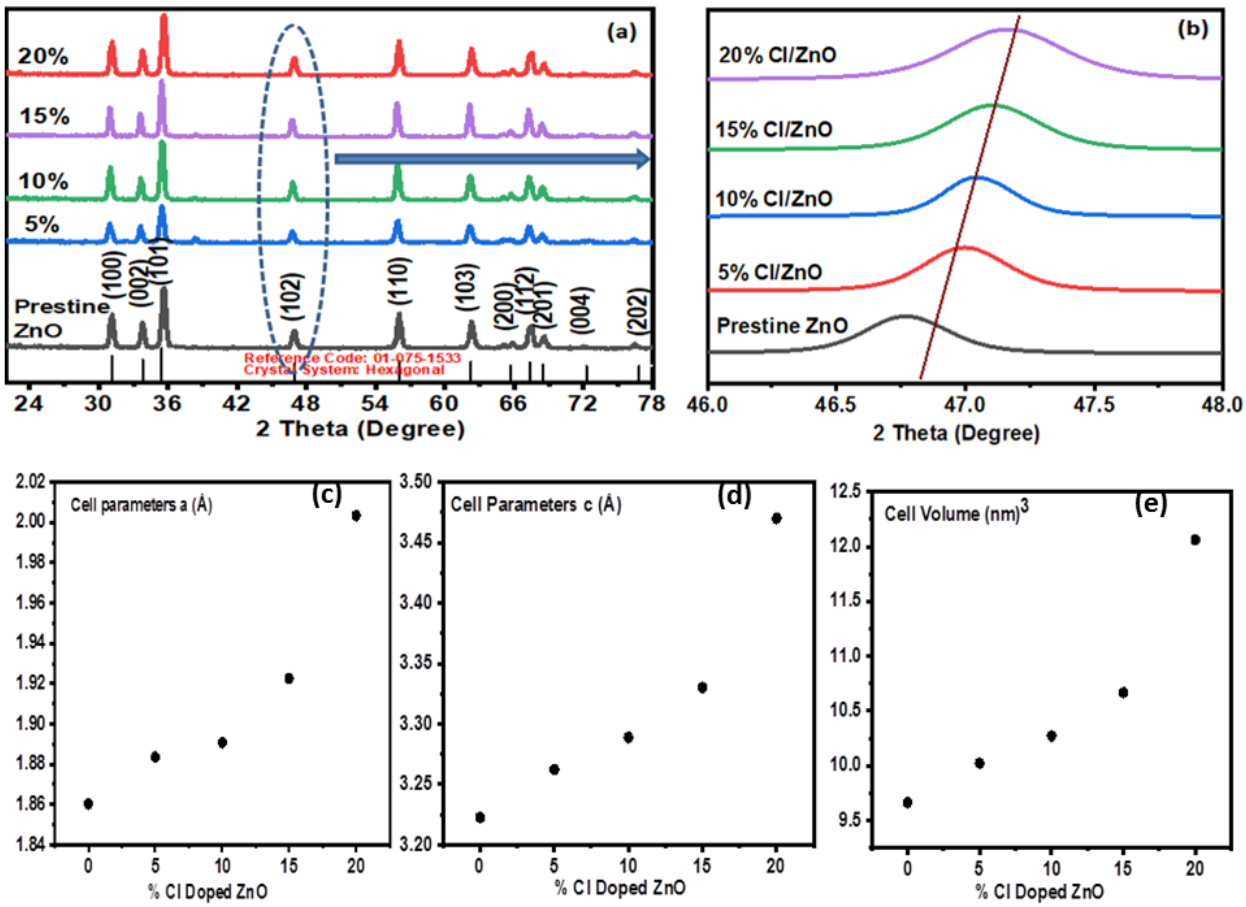

Figure 2(a) XRD patterns for pure and Cl^- -doped ZnO nanostructures, which can be indexed as a single phase of wurtzite ZnO structure using referencing code: (01-075-1533). **(b)** The observed increasing shift in peak at 2Θ angle of 47.452 degree. (**c-e**) shows cell parameters a, c and cell volume of ZnO:Cl nanostructures.

This increasing order may be justified owing to larger ionic radius of Cl^- (r = 1.81Å) compared with O^{2-} (r = 1.40 Å) and this leads to the induction of consistent expansion of the ZnO lattice structures [46]. In addition, the doping of Cl^- into ZnO can further alter the distance in crystal structure as well as in diffraction angle. Moreover, the crystallite size of the as-prepared samples was evaluated from Scherer's relation [47].

$$D(nm) = \frac{K\lambda}{(FWHM)_{hkl}\, Cos(\Theta)} \quad (2)$$

Where D is crystalline size (nm), shape factor K= 0.94, λ shows wavelength of X-Ray (nm), **β** depicts Full Width at Half Maximum (rad) Θ denotes Bragg Diffraction Angle (deg). The average value of crystalline size of synthesized nanostructures was found 23.356 nm and

their values were obtained in decreasing order with increasing Cl^- as a dopant concentration into ZnO. The decreasing order from (30.26 to 13.66 nm) in crystallite size is most likely to be a contribution from the diffused and grown aspect of ZnO crystal structure due to marked difference in ionic radius between Zn^{2+} (0.74 Å) and Cl^- (1.8 Å), respectively. The chloride ion as counter ion with other metal ions have shown reduction in the crystallite size due to difference in the ionic radii of metallic ion and the chloride ion itself [48]. These size characteristics are essential parameters for possibly improving the photocatalytic properties of Cl^--doped ZnO nanostructures for potential applications in wastewater treatment as well as clean up the environment. These crystallographic values of the as-synthesized nanostructures are summarized in Table 1.

Samples	FWHM (degree)	Crystalline Size (nm)	a(Å)	c(Å)	c/a(Å)	d-spacing (nm)	Volume $(nm)^3$
Pristine ZnO	0.388	30.23	1.86	3.22	1.73	0.80	9.66
5%Cl/ZnO	0.376	27.23	1.88	3.26	1.73	0.81	10.02
10%Cl/ZnO	0.381	25.27	1.89	3.28	1.73	0.82	10.27
15%Cl/ZnO	0.425	20.54	1.92	3.33	1.73	0.83	10.66
20%Cl/ZnO	0.542	13.66	2.00	3.47	1.73	0.86	12.06

Table 1: Lattice parameters, broadening width at half maximum, crystalline sizes d-spacing, Volume of synthesized pristine and Cl- -ZnO nanostructures

Scanning electron microscopic (SEM) analysis revealed that the addition of Cl^- ion as a dopant into ZnO has significantly altered the morphology and crystal size from nanorod to approximately thin film like structure. As can be evident from Fig. 3a, the pristine ZnO has short nanorods morphology with hexagonal facets. The addition of 5% Cl^- source as a dopant into the ZnO precursors resulted in almost the same nanorods like morphology, but having randomly aligned as shown in Fig. 3b. Further addition of 10% Cl^- -dopant into ZnO precursor yielded a slightly aggregated structure with the presence of few nanorods (Fig. 3c). Upon

addition of 15% Cl^- dopant, compact cluster of nanorods has been produced (Fig. 3d). Finally, the addition of 20% Cl^- as a dopant into ZnO precursor gave rise to a diffused and thin film like morphology with some of the nanorod like features as shown in Fig. 3e.

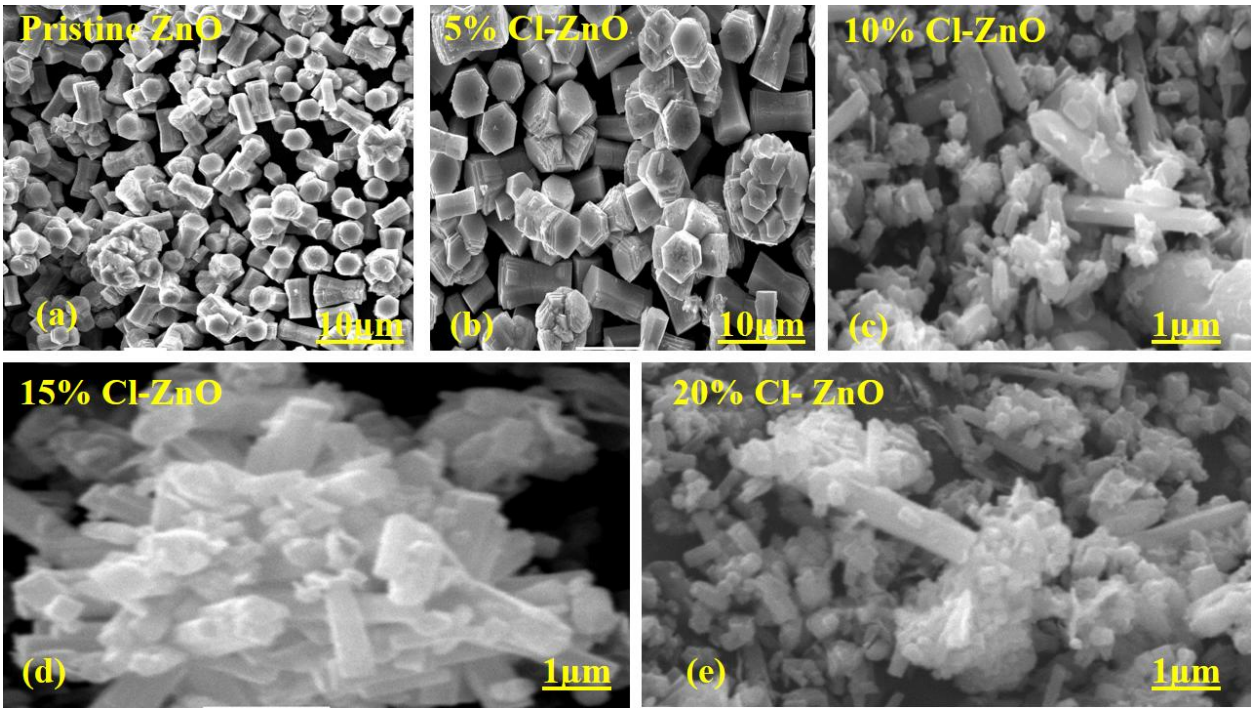

Figure 3 (a-e) pristine ZnO, 5, 10, 15, and 15% Cl^- doped ZnO respectively.

The EDX was employed to quantitatively analyze the presence of zinc, oxygen and chlorine in the as-synthesized pristine ZnO and Cl^- -doped ZnO samples and spectra are enclosed in Figure 4 (a-e). Closer inspection of the obtained EDX pattern clearly emphasized that undoped ZnO peaks, appeared in the emission of X-rays, only related to zinc and oxygen atoms as illustrated in Fig. 4(a). Figures 5(b-e) obtained for 5%, 10%, 15% and 20% Cl^- -doped ZnO, respectively showed the presence of chlorine atom along with zinc and oxygen atoms. Thus, the combined EDX data confirmed the successful incorporation of Cl^- into ZnO nanostructured. The weight percentage of chlorine was obtained as 0.62%, 1.77%, 2.93%, and 3.675% in the 5%, 10%, 15% and 20% Cl^- -doped ZnO samples, respectively.

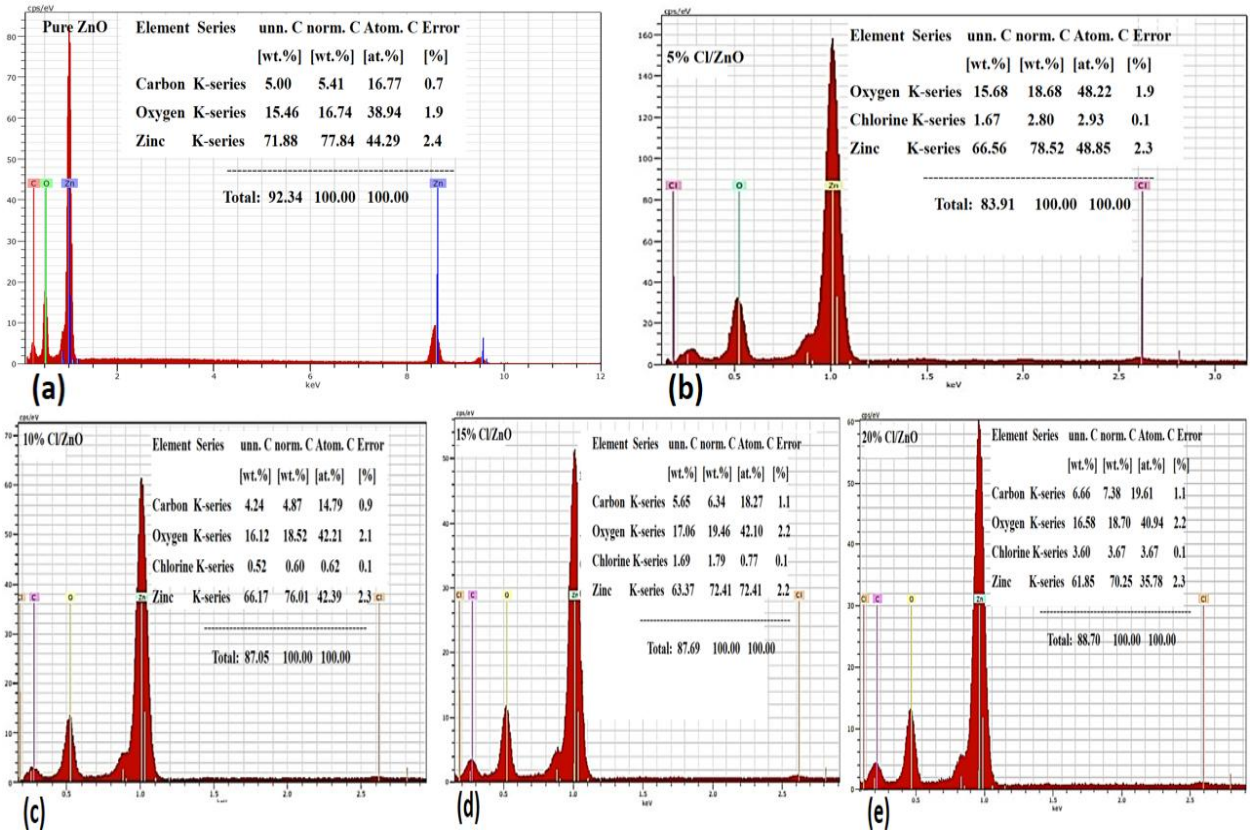

Figure 4 (a) depicts the elemental composition of undoped ZnO and **(b-e)** shows ingredients in 5%, 10%, 15%, and 20% Cl^- doped ZnO.

Exploring the optical features of both pure ZnO and the four different samples of the as-prepared Cl^--doped ZnO nanostructures was undertaken via UV-Vis spectroscopy. Figure 5 represents the absorbance spectra measured over the range of 200 to800 nm. Careful analysis of the obtained spectra implied that increasing Cl^- ion concentration by 5%, 10%, 15% and 20% causes maximum wavelength absorption shift to higher wavelength, which could be assigned to agglomeration of the nanostructures as reported elsewhere [49]. The energy gap conduction band (CB) and valence band (VB) may be assigned to optical band gap, E. For hydrothermally synthesized photocatalysts, the Tauc-equation is used to calculate band gap energy (E_g)

$$(\alpha h\nu)^n = k(h\nu - E_g) \quad (3)$$

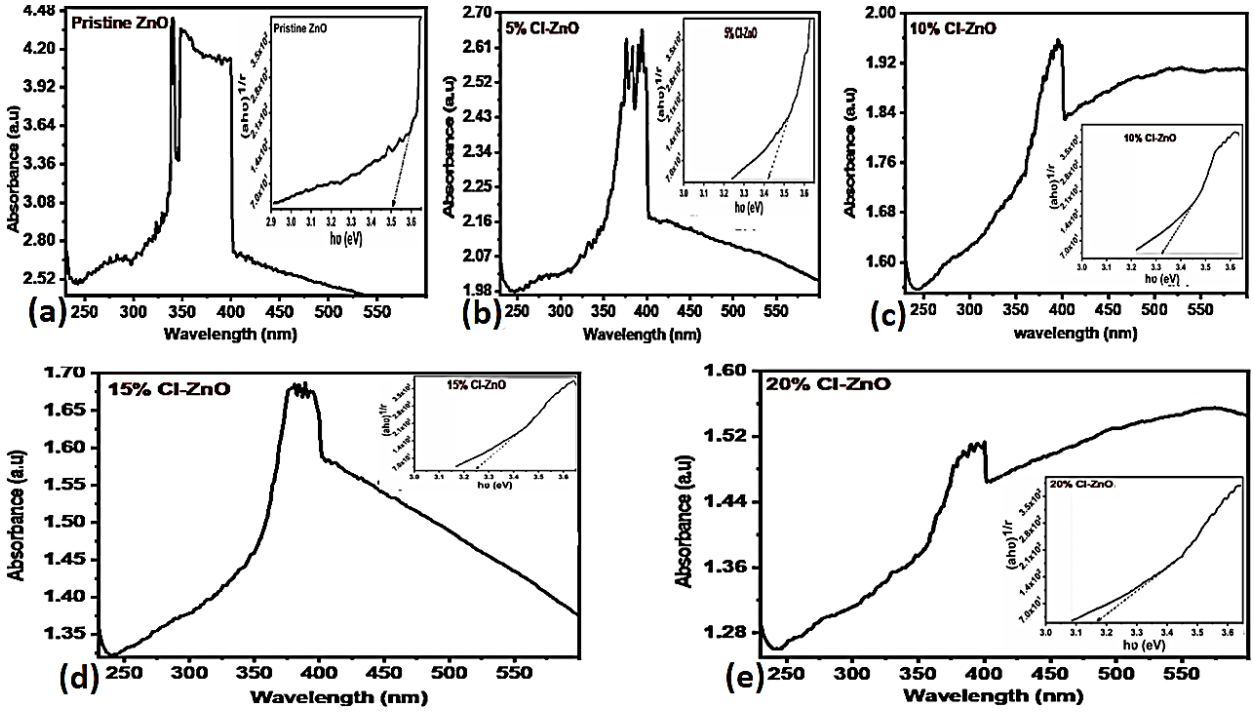

Figure 5(a) depicts the UV absorption spectrum and inset shows the Tauc plot between energy and $(\alpha h\nu)^2$ for Pristine ZnO. The extrapolation in inset represents 3.51 eV of pristine ZnO, **5(b-e)** represents UV absorption spectra and their insets show the Tauc's plot between energy and $(\alpha h\nu)^2$ for 5%, 10%, 15%, and 20% Cl^--doped ZnO, respectively.

\Where α denotes absorption coefficient, K is constant, hν is photon energy, n = 2 and E_g (e.V) represents the energy of optical band gap. Tauc's plots of ZnO and Cl^- -doped ZnO are represented in Figures 5(b-e). The insets in Figures 5(b-e) reveal the linear relation between $(\alpha h\nu)^2$ and hν and this linear portion of Tauc's plot was extrapolated to the ordinate as to be equal to 3.54 eV. The band gap energies of Cl^- -doped ZnO were evaluated as 3.42, 3.32, 3.24, and 3.16 eV for 5%, 10%, 15% and 20% Cl^- -ZnO, respectively. The band gap energy follows slightly decreasing order owing to density of defects between the conduction band and valence band of Cl^- -ZnO, which possibly arises from the Cl doping into ZnO. Thus, the non-metal (Cl) doped ZnO causes decrease in optical band gap energy, which indicates the potential of Cl^- -ZnO nanostructures under UV light irradiation. The extrapolations in their insets represent 3.42, 3.32, 3.24, and 3.16 eV for 5%, 10%, 15%, and 20% Cl^- -ZnO, respectively

3.2. Photodegradation activity of Cl^- doped ZnO nanostructures

The photodegradation of (MB) using pristine ZnO and Cl^--doped ZnO nanostructures was performed by irradiating UV light. The UV-Vis spectra of MB in aqueous solution at different pH values were recorded at different irradiation time intervals of 25 min for pure ZnO and 15 min for Cl^- -ZnO as presented in Figures 6(a, b). Photodegradation activity of Cl^--doped ZnO nanostructures samples were inspected by pseudo-first order and linearly fitted graph Ln (C_o/C_t) versus time showing degradation rate as enclosed in Figures 6(c, d), respectively.

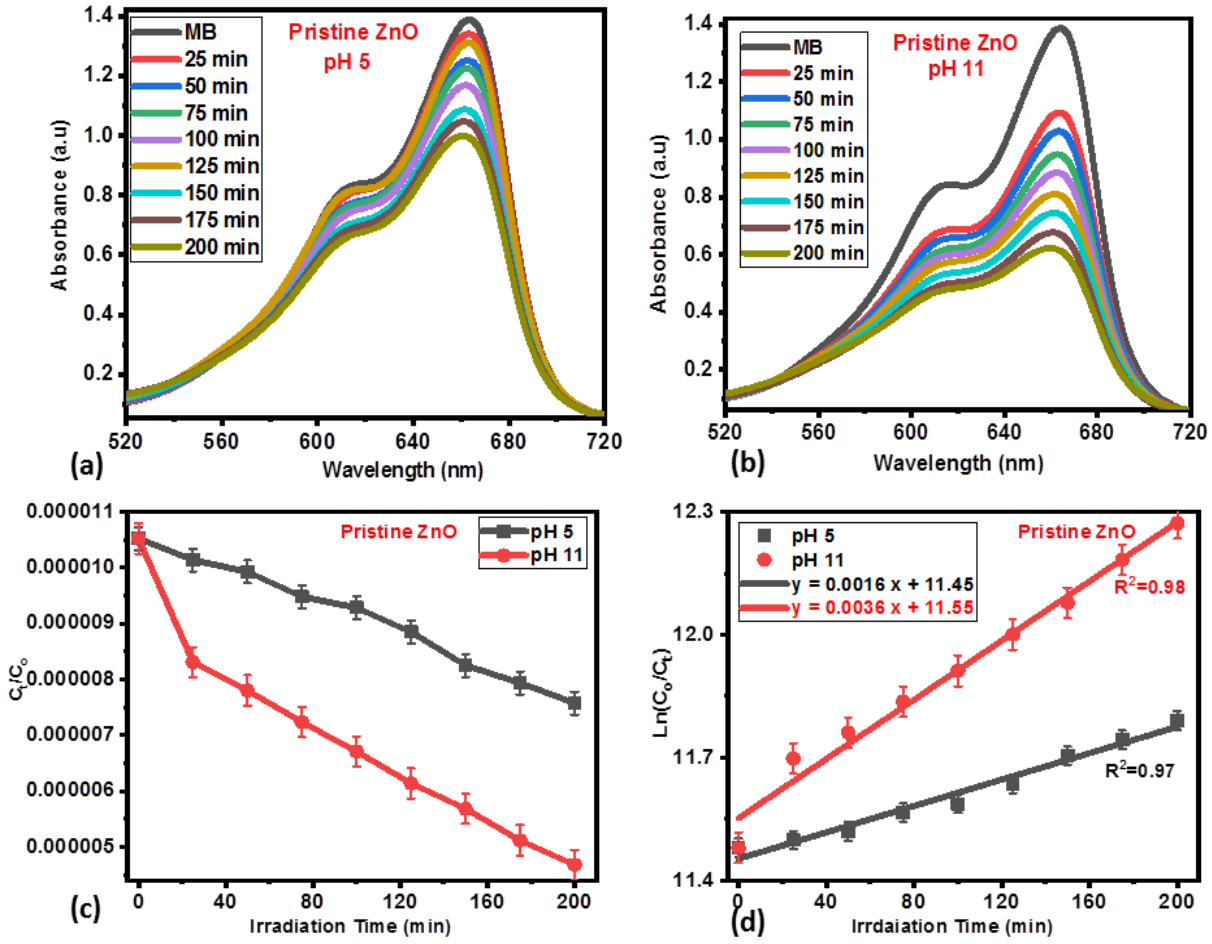

Figure 6 (a, b) UV-Vis absorbance spectrum of MB at certain intervals for pristine ZnO at pH 5 and pH 11 **(c)** depicts C_t/C_o versus time **(d)** linearly fitted graph Ln (C_o/C_t) versus time showing degradation rate

The maximum absorbance peak in the spectra was measured at 664 nm. The decreasing height of the absorbance peak at 664 nm is a function of irradiation time as shown in Figures 7 and 8, thereby reflecting the degradation of MB dye at pH 5 and 11.

The illumination of UV light on the surface area of ZnO and Cl^--doped ZnO nanostructures causes photogeneration of electron–hole pairs between conduction and valence bands, which is generally responsible for the ignition of photocatalytic decomposition process leading to degradation of dye pollutant. The photo-exited electron goes to CB where it offers high oxidation potential to allow direct oxidation of MB in reaction medium. Furthermore, the photogenerated species in VB and in CB limits the recombination rate of electron and hole by following the oxidation reaction with either H_2O, OH^- or O adsorbed on ZnO and Cl^-doped ZnO to produce the hydroxyl radicals through the following reactions [50, 51]:

$$Cl - ZnO + hv \rightarrow e_{CB}^- + h_{VB}^+ \quad (4)$$

$$e_{CB}^- + O_{2(adsorbed)} \rightarrow O_2^{\bullet} \Rightarrow 2O_2^{\bullet -} + H^+ \rightarrow H_2O^{\bullet -} + O_2^{\bullet -} \quad (5)$$

$$h_{VB}^+ + H_2O \rightarrow H^+ + HO^{\bullet} \quad (6)$$

$$e_{CB}^- + h_{VB}^+ \rightarrow Cl - ZnO + Heat \quad (7)$$

$$H_2O_2 + e_{CB}^- \rightarrow HO^{\bullet} + OH^- \quad (8)$$

$$H_2O_2 + O_2^{\bullet -} \rightarrow HO^{\bullet} + OH^- + O_2 \quad (9)$$

$$H_2O_2 + hv \rightarrow 2HO^{\bullet} \quad (10)$$

Finally, the hydroxyl radicals are used as the scavengers to decompose MB dye pollutant through following reactions [51].

$$Dye + (O_2^{\bullet -} \rightarrow HO^{\bullet} + HO_2^{\bullet}) \rightarrow Intermediate \rightarrow Product \quad (11)$$

Figure 6 (a, b) schematically depicts the slow decreasing of the MB with time of 200 min at pH 5 and 11, whereas in case of Cl^- -doped ZnO the decrease in the height of the absorbance peak occurs much faster with almost complete degradation of MB within irradiation time of 90 min at pH 5 and 11 as illustrated in Figures 7 (a-d) and 8 (a-d), respectively.

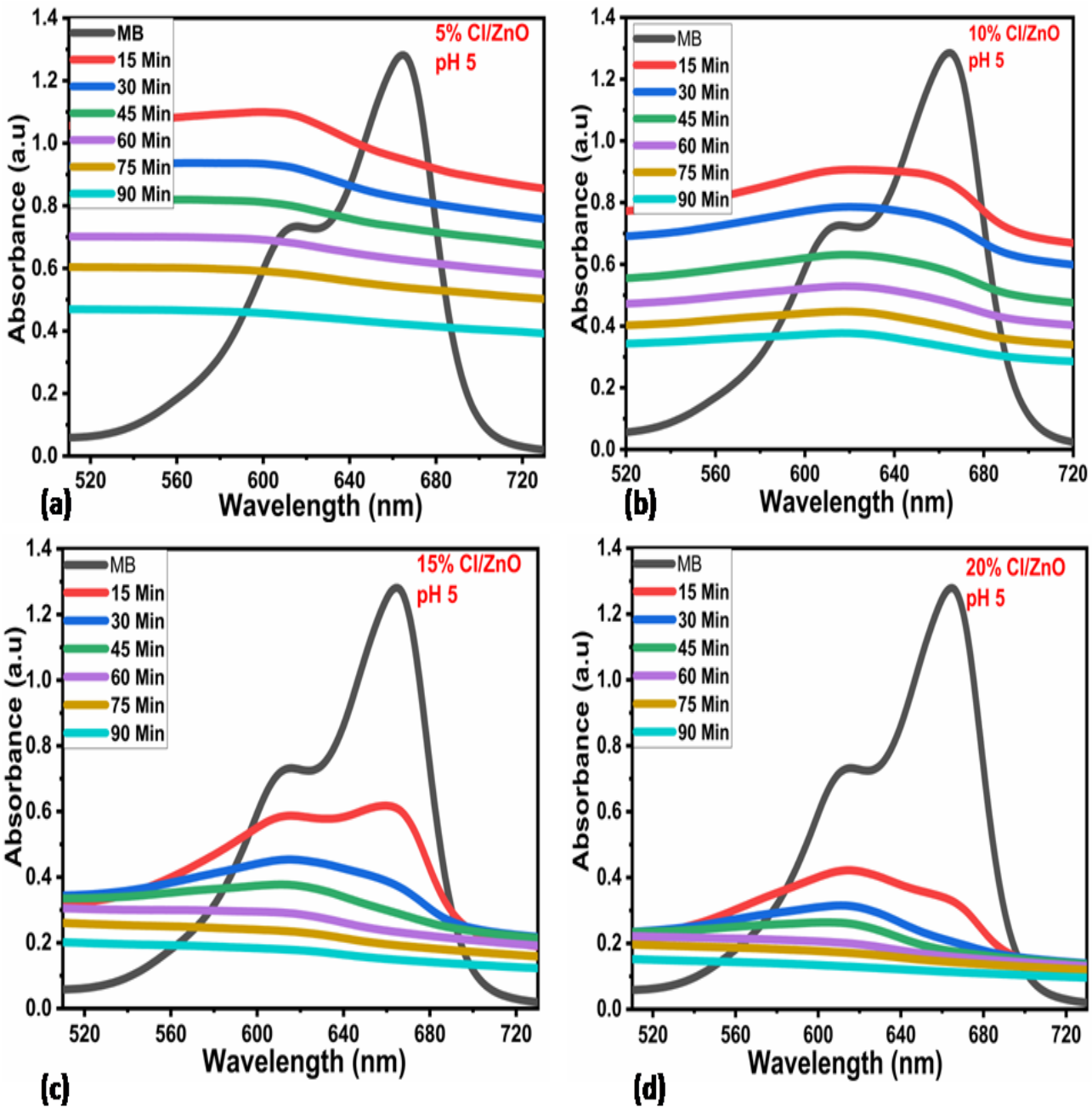

Figure 7(a-d) UV-Vis absorbance spectra monitoring the concentration of MB after 15 intervals of time for 5%, 10%, 15% and 20% Cl^- -ZnO at pH 5, respectively.

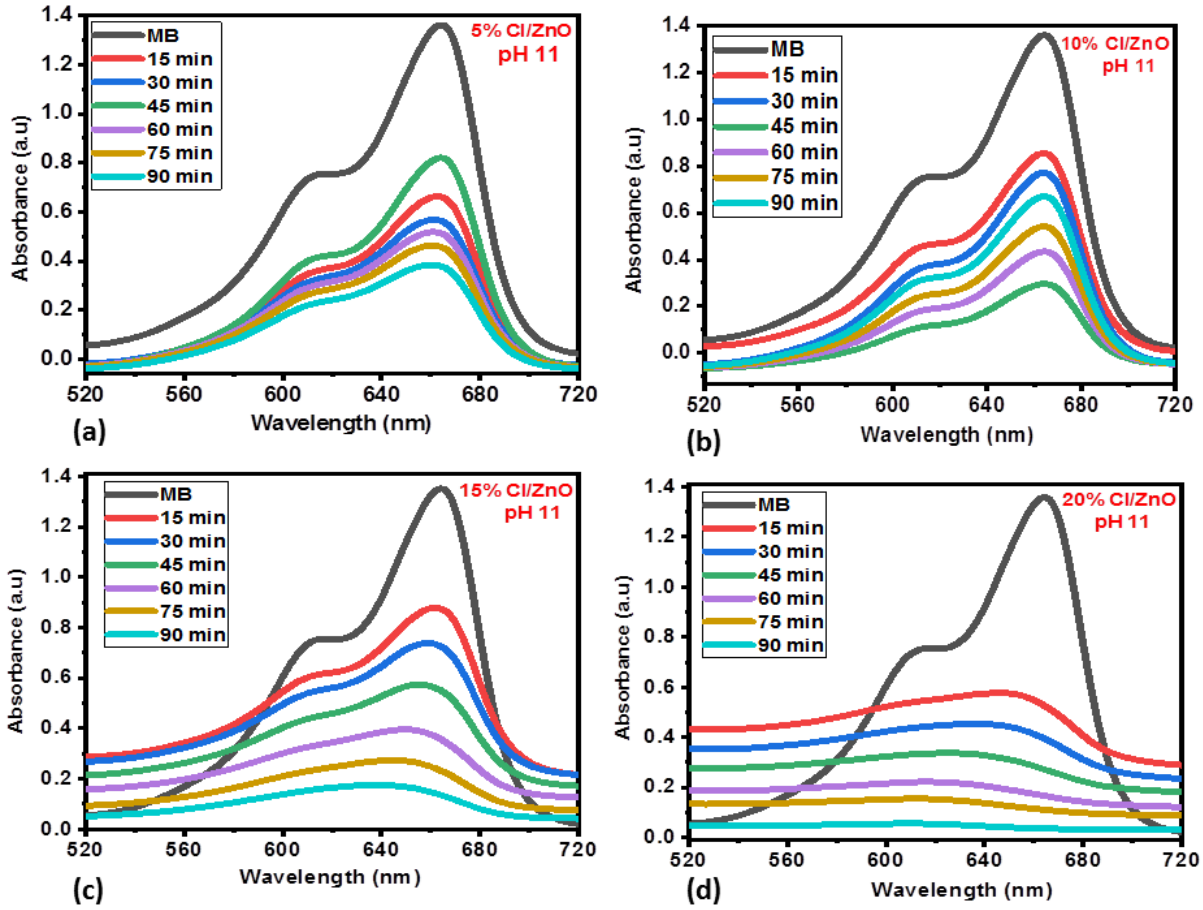

Figure 8 (a-d) UV-Vis absorbance spectra monitoring the concentration of MB after 15 min intervals of time for 5%, 10%, 15% and 20% Cl^--doped ZnO at pH 11, respectively.

The photocatalytic degradation activity may also be affected by various factors such as amount of catalysts, pH value, and concentration of MB, radiation of energy as well as the irradiation time. The effect of concentration of Cl^- as a dopant into ZnO on the photodegradation of MB dye was investigated using different samples of Cl^- -doped ZnO photocatalyst. For this study, percentile of Cl^- as a dopant was varied from 5% to 20% of ZnO to optimize the performance of the photocatalysts. The 0.1 mM concentration of MB dye was kept constant for all samples to evaluate the effect of dopant concentration on the degradation process. The obtained data reveals that photocatalytic degradation efficiency for MB with pristine ZnO was about 57.75% and 75.78% over 200 min at pH of 5 and 11, respectively, as shown in Figure 9(a). Whereas, the performance with 5%, 10%, 15%, and 20% Cl^- -doped ZnO over a period of 90 min was calculated to be 64.47%, 71.35%, 80.03% and 89.91%, respectively at pH 5 (see Fig. 9(b)).

These values are markedly enhanced upon increasing the pH to 11, where under the same reaction time (90 min) about 75.20%, 81.19%, 88.67% and 99.45% were achieved as shown in Fig.9(c). In view of these results, it is clearly established that with 20% Cl^- concentration in ZnO the best photocatalytic activity for MB degradation with efficiency of ~89.91% and 99.47% within 90 min was attained at pH values of 5 and 11, respectively as represented in Fig.9 (b, c). This improved photocatalytic performance with 20% Cl^- -dopant ZnO could be attributed to the presence of surface- active sites and reduction in the optical band gap [52]. Thus, it can be concluded that 20% Cl^- -doped ZnO is giving maximum degradation efficiency and hence it may be considered as a promising photocatalyst for wastewater treatment..

It is widely accepted that the pH of a stock solution can be considered as a main factor and plays a vital role in driving the photosensitivity of material through the surface charges [53, 54]. For this purpose, we studied the effect of pH on the photosensitivity of as-prepared Cl^-doped ZnO materials towards the degradation of MB at pH 5 and 11. The pH value was set with help of 0.1 M HCl and 0.1 M NaOH. The MB concentration of 0.1 mM was kept constant. In this study, we found that the photocatalytic efficiency of pure ZnO (without Cl^- doping) is ~50% and 55% at pH 5 and 11, respectively. The degradation efficiency of pristine n-type semiconductor ZnO was evaluated to be 57.75% and 75.78% over the time intervals of 200 min at pH 5 and 11, respectively as shown in Fig: 9(a). Whereas, Figure 9(b) shows under same time and same condition the 20% Cl^- -doped ZnO could degrade 89.91% at pH of 5 indicating degradation efficiency at pH 5 is less than pH 11. On other hand, with 20% Cl^--doped ZnO, the photocatalytic efficiency reached maximum at pH of 11 with degradation efficiency of 99.47% of MB over 90 min for 20% Cl^- -doped ZnO as represented in Figure 9(c). On the basis of this finding, it is evident that the degradation reaction is highly accelerated in alkaline media compared to acidic; this might be due to the greater electrostatic attraction between MB and the nanocomposites [55, 56]. The minimum efficiency was observed at pH 5 and 11 for 5% Cl^- -doped ZnO with degradation efficiency of 64.92% and 75.23%, respectively as presented in Figure 9(b, c). The obtained results of degradation efficiency are very close to the previous studies.

Figure 9: (a) Degradation efficiency of pristine ZnO at pH 5 and 11 **(b)** Degradation efficiency of Cl-ZnO nanostructures at pH 5 **(c)** Photodegradation Efficiency of Cl^- -ZnO nanostructures at

pH 11 **(d)** Degradation rate ~~coefficient~~ with Cl^- increasing percentile concentration with ZnO at pH 5 and 11

research work [56]. The role of pH on the photosensitivity of material is complicated and could be understood through the related reported works [57]. Additionally, S. Sunitha *et al*, [58], Iraj Kazeminezhad *et al*, [59] have proposed that both the acidic and basic features on the surface of the metal oxides as well as the density of zero-point charge (zpc) can be considered as the main factors for producing lower photocatalytic degradation performance at lower pH values and higher degradation efficiency at higher pH values.

The photocatalytic activity of pristine ZnO and Cl^--doped ZnO for the degradation of MB solution was evaluated under UV light. The evaluation in terms of quantifying the differences in degradation rates and obtaining the pseudo first-order kinetic constants was accomplished via using MB solution. Moreover, the rate of photocatalytic reaction and MB photo-decolorization rate constants have been performed using pseudo first order kinetics as shown in the following equation.

$$Ln\frac{C_o}{C_t}=Kt \tag{12}$$

Where, C_o concentration of MB before degradation, C_t concentration of MB after degradation of at time (t), k shows Pseudo-first order rate constant. The degradation rate coefficient was obtained through the linear fitting of Ln (C_0/C_t) as a function of time. The degradation rate was highly enhanced with successive addition of Cl^- concentration into ZnO. Figure 5d shows the linearly fitted kinetic plot between $Ln\frac{C_o}{C_t}$ and time interval (min) yielding the degradation rate ~~coefficient~~ for pristine ZnO at pH 5 and 11. The linearly fitted kinetic plot follows the pseudo first order kinetics model and operating the slope may yield the degradation rate constant of 0.004 min^{-1} and 0.006 min^{-1} at pH 5 and 11, respectively as shown in Figure 6(d). Whereas in the case of Cl^- -doped ZnO, a better degradation rates for MB at pH 5 and 11 were attained. Figure 10 (b and d) depicts the linearly fitted graph between $Ln\frac{C_o}{C_t}$ and time (min) revealing the degradation rate constants are function of Cl^- ion concentration with respect to ZnO at pH 5 and 11, respectively.

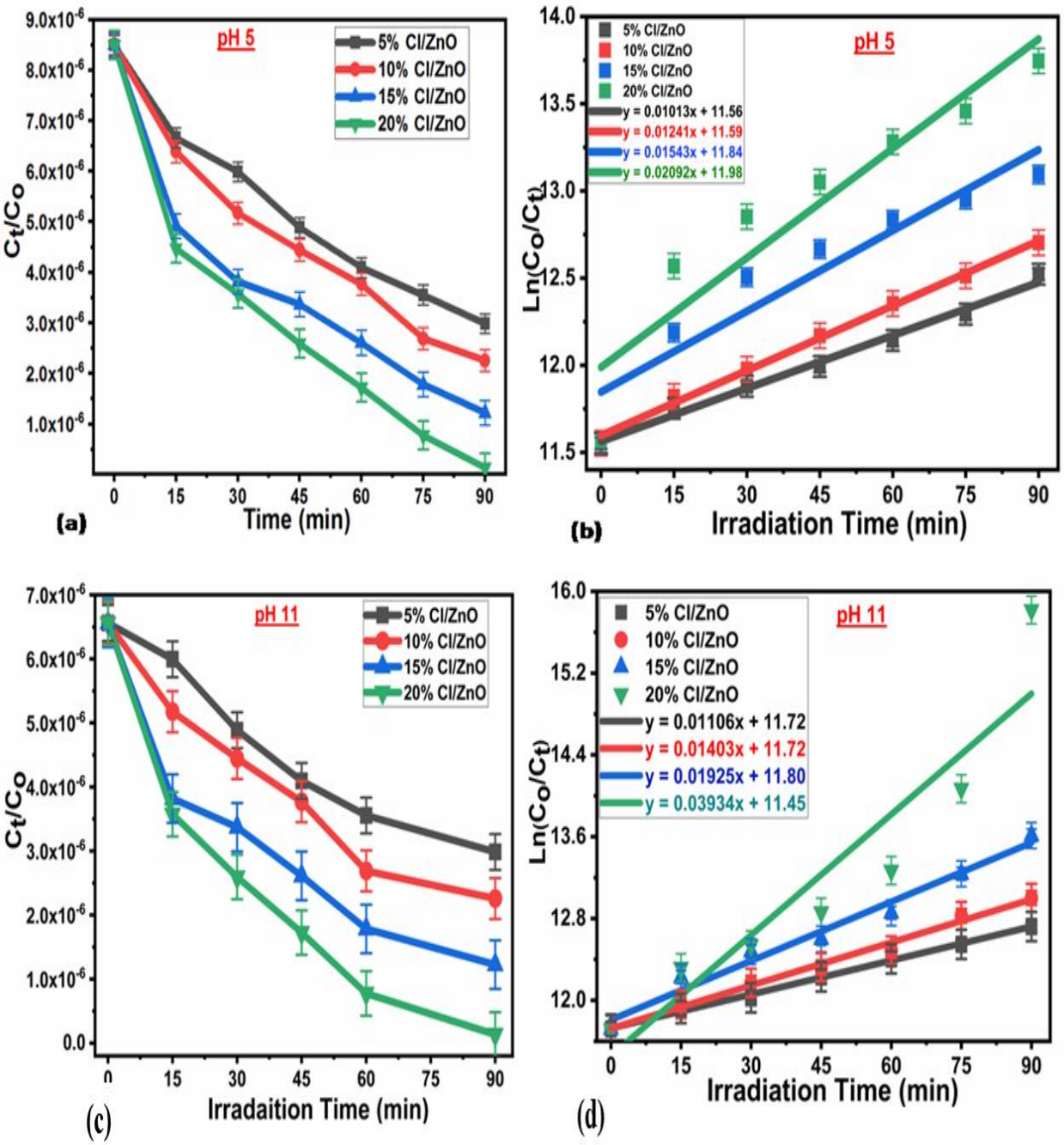

Figure 10 (a and **c)** Depicted graph C_t/C_o versus time, indicating decreasing trend for 5%, 10%, 15% and 20% Cl^- -doped ZnO at pH 5 and11, whereas Figure 10 **(b** and **d)** represented the linearly fitted graph Ln (C_o/C_t) versus time and showing increasing degradation rate for 5%, 10%, 15% and 20% Cl^- -doped ZnO at pH 5 and 11, respectively.

As more Cl ions appears on the surface of ZnO, it causes slower recombination rate which ultimately leads to a faster degradation rate at both pH 5 and 11 [60]. Moreover, the doping of Cl^- into solid ZnO may increase the escaping of number of electrons/holes pairs to the surface of ZnO nanostructures and therefore enhanced photodegradation rate and efficiency of the Cl^--doped ZnO. The estimation parameters such as degradation rate, pH value, degradation efficiency, time, optical band gap and regression coefficient (R^2) are listed in Table 2.

Table 2: shows time for degradation, degradation efficiency, R^2 and rate constant at pH 5 and 11.

Samples	Band Gap (eV)	pH 5				pH 11			
		Time (min)	Deg: Eff: (%)	R^2	Rate constant (min^-1)	Time (min)	Deg: Eff: (%)	R^2	Rate constant (min^-1)
Pristine ZnO	3.54	200	57.56	0.99	0.004	200	75.78	0.97	0.006
5%Cl/ZnO	3.42	90	64.47	0.98	0.010	90	75.20	0.97	0.012
10%Cl/ZnO	3.32	90	71.35	0.97	0.014	90	81.19	0.98	0.015
15%Cl/ZnO	3.24	90	80.03	0.95	0.018	90	88.67	0.97	0.018
20%Cl/ZnO	3.16	90	89.91	0.93	0.021`	90	99.45	0.91	0.041

It is worth mentioning here that the increase in the Cl^- as a dopant concentration, from 5 to 20%, has caused a gradual change in degradation rate, from 0.010 to 0.021 min^{-1} at pH 5, whereas at pH 11 it increases from 0.012 to 0.041 min^{-1} as shown in Figure 9(d).

The maximum photocatalytic activity was measured at 20% Cl^--doped ZnO over pH 5, with a degradation rate five times larger than that of pristine ZnO. On the other hand, with 20% Cl^--doped ZnO, it appeared six times larger than that of pristine ZnO at pH 11. Thus, the two-fold approaches were reported for the cause of the improved photocatalytic performance. First, it might be assigned to the combinational effect of Cl^- and ZnO. It was noticed by the reduction of size and optical band gap of prepared Cl^- doped ZnO samples, which consequently led to the suppression of the recombination of electrons/holes pairs [49]. In other words, in a particular system, the rate of interfacial charge transfer may be increased by decrease in particle size, which consequently increases the number of active surface sites. In this case, hydroxyl and

superoxide radicals are formed when the photogenerated charge carriers react with absorbed molecules. However, our findings revealed that the decrease in the particle size might not sole responsible for the improved photocatalytic activity. The rate of degradation of MB might be affected by the amplification in the rate of recombination process, thus sufficiently small particle in size is proportionally raising the activity [61]. In addition, the degradation rates for Cl^--doped ZnO follows an order of 20% Cl^--doped ZnO > 15% Cl^--doped ZnO > 10% Cl^--doped ZnO > 5% Cl^--doped ZnO at both pH values of 5 and 11.

Additionally, pH 11 yields the optimum photo degradation activity giving rise to a degradation rate of 0.041 min^{-1}. Significantly, the maximum values at pH 5 and 11 are in good agreement with the reported literature and the obtained results are justified with the dynamic approach in which increasing the pH of the medium may cause creation of more available active sites and thereby yielding more hydroxyl radicals onto the catalyst surface [61]. Besides, the decreasing trend in band gap energy influences the photocatalytic performance for waste water treatment. Our findings regarding band gap appeared in decreasing order, from 3.54 to 3.16, with increasing Cl^- concentration into ZnO. As band gap findings suggest that a decrease in the band gap energy can produce enhanced performance of Cl^--doped ZnO at both pH 5 and 11. The peak performance obtained with 20% Cl^--doped ZnO was 89.91% and 99.45% at pH 5 and 11, respectively as shown in Figure 9(b, c). Significantly, the prepared Cl^--doped ZnO nanostructures, in this investigation, showed a much greater efficiency in the degradation process of MB upon exposure to UV light than previous studies as summarized in Table 2. The degradation efficiency of the synthesized pristine ZnO and Cl^--doped ZnO for removal of MB over pH 5 and 11 is as follows: ZnO < 5% Cl^--doped ZnO < 10% Cl^-- doped ZnO < 15% Cl^--doped ZnO < 20% Cl^-- doped ZnO. Thus, the 20% Cl^--doped ZnO might be considered as the optimum value for a promising photocatalysts [62].].

Furthermore, this observation may be also explained as that introducing of various concentration of Cl^- ions as dopant into ZnO nanostructures may lead to large plasmonic effect that produces significant impact on reaction kinetics and degradation efficiency. The degradation efficiency of proposed study at pH 5 and 11 was compared with the published works [63-70] as given in Table 3. It is obvious that the our Cl doped ZnO material has either equal or superior degradation efficiency in highly alkaline conditions. The possible reason of higher performance in high alkaline pH of dye solution could be related to the high density of hydroxyl groups which

potentially improved the degradation reaction kinetics of MB in aqueous solution, consequently higher degradation efficiency was observed.

Table 3: Shows the comparison of degradation efficiency of the 20% Cl^-doped ZnO photocatalyst at pH 5 and 11 with the reported results.

Name of Material	**Light source**	**Dye**	**pH**	**Catalyst Dose**	**Time**	**Degradation Efficiency**	**Ref**
ZnO	UV light	MB	11	…….	240 min	81%	[63]
W-ZnO	UV light	MB	11	20mg	90 min	89%	[64]
ZnO	UV light	MB	11	0.05g	240 min	81%	[56]
Mn-ZnO	UV light	MB	05	0.30g/L	120 min	41%	[65]
WO3/SiO2	UV light	MB	11	0.1 g/L	120 min	91%	[66]
ZnS:CdS	UV light	MB	10	0.1g/L	360	73%	[67]
ZnO/SAPO-34 (AC-U)-U	Sunlight	MB	6	1g/L	150 min	95.7%	[68]
Ag/ZnO	UV light	MB	8	3g/L	180 min	100%	[69]
$ZnO/Eu_2O_3/NiO$	UV light	MB	10	0.03g/L	150 min	98	[70]
Cl^--doped ZnO	**UV light**	**MB**	**05**	0.1g/L	**90 min**	**89.91%**	**Present Work**
Cl^--doped ZnO	**UV light**	**MB**	**11**	0.1g/L	**90 min**	**99.45%**	

4. Conclusions

In summary, we have successfully synthesized four new Cl-doped ZnO samples having 5, 10, 15, and 20% concentrations of Cl^- ion and compared its photocatalytic degradation efficiency towards MB at acidic (pH = 5) and basic (pH=11) media to that of pristine ZnO. The effect of pH on degradation of MB as well as the role of different concentration of Cl^- as dopant into ZnO was investigated. The obtained results for the band gap energy of all Cl-doped sampled were found in decreasing trend whereas the efficiency of photocatalytic degradation of MB was observed in increasing trend. The doping of Cl- ion induced the reduction of optical band gap of ZnO, created defects in the crystal structure and consequently enhanced photocatalytic activity towards the degradation of MB in alkaline conditions was observed. The obtained maximum degradation constants were (0.021 min^{-1}), (0.041 min^{-1}), five and six times larger than that of pristine ZnO, at pH 5 and 11, respectively for the 20% Cl^--dopedZnO. Upon irradiation for ~200 min, the degradation efficiency of pristine ZnO was found to be 57.75% and 75.78% at pH 5 and 11, respectively, whereas much higher values of 89.91% and 99.45% were obtained for he 20% Cl^--doped ZnO after irradiating with UV light for only 90 min. The photocatalytic efficiency upon using Cl^--doped ZnO nanostructures for degradation of MB was observed in the order (20% Cl^--doped ZnO > 15% Cl^-- doped ZnO > 10% Cl^-- doped ZnO > 5% Cl^-- doped ZnO > pristine ZnO). The obtained results confirm that the Cl^- doped ZnO nanostructures may be considered as a promising and alternative photocatalysts for wastewater treatment and other related environmental applications.

Acknowledgment

We extend our sincere appreciation to the Researchers Supporting Project (RSP-2022/265) at King Saud University, Riyadh, Saudi Arabia for partial funding of this work.

Conflict of interest statement

Authors declare there are not conflict of interest in this research work.

7. References

[1] Chikkanna, M.M.; Neelagund, S.E.; Rajashekarappa, K.K. Green synthesis of zinc oxide nanoparticles (ZnO NPs) and their biological activity. SN Applied Sciences. 2019, 11-0.

[2] Çiçek, F.; Özer, D.; Özer, A.; Özer, A. Low cost removal of reactive dyes using wheat bran. Journal of Hazardous Materials. 2007, 146, 408-416.

[3] Aboamera, N.M.; Mohamed, A.; Salama, A.; Osman, T.A.; Khattab, A. An effective removal of organic dyes using surface functionalized cellulose acetate/graphene oxide composite nanofibers. Cellulose. 2018, 25, 4155-4166.

[4] Mohamed, A.B.; Eleuch, H. Generation and robustness of bipartite non-classical correlations in two nonlinear microcavities coupled by an optical fiber. JOSA B, 2018, 35, 47-53.

[5] Tolia, J.; Chakraborty, M.; Murthy, Z.V. Photoluminescence of photocatalytic degradaded malachite green dye by using Mn-doped ZnS. In 2011 International Conference on Biology, Environment and Chemistry IPCBEE. 2011, 24.

[6] Lee, K.M.; Lai, C.W.; Ngai, K.S.; Juan, J.C. Recent developments of zinc oxide based photocatalyst in water treatment technology: a review. Water research. 2016, 88, 428-448.

[7] Crini, G.; Lichtfouse, E.; Wilson, L.D.; Morin-Crini, N. Conventional and non-conventional adsorbents for wastewater treatment. Environmental Chemistry Letters. 2019, 17, 195-213.

[8] Baruah, S.K.; Pal, S.; Dutta, J. Nanostructured zinc oxide for water treatment. Nanoscience & Nanotechnology-Asia. 2012, 2, 90-102.

[9] Konstantinou, I.K.; Albanis, T.A. Photocatalytic transformation of pesticides in aqueous titanium dioxide suspensions using artificial and solar light: intermediates and degradation pathways. Applied Catalysis B: Environmental. 2003, 42, 319-335.

[10] Farouq, R. Investigation of the kinetics and optimization of photocatalytic degradation of methylene blue. *Journal of the Chinese Chemical Society*. 2018, 65, 1333-1339.

[11] Rafaie, H. A.; Nor, R. M,; Azmina, M. S.; Ramlia, N.I.T.; and Mohamed R. J. Environ. Chem. Eng. 2017, 5, 3963.

[12] Kołodziejczak-Radzimska, A.; Jesionowski, T. Zinc oxide—from synthesis to application: a review. *Materials*. 2014, 7, 2833-2881.

[13] Kiwaan, H.A.; Atwee, T.M.; Azab, E.A.; El-Bindary, A.A. Efficient photocatalytic degradation of Acid Red 57 using synthesized ZnO nanowires. Journal of the Chinese Chemical Society. 2019, 66, 89-98.

[14] Wang, J.; Cao, J.; Fang, B.; Lu, P.; Deng, S.; Wang, H. Synthesis and characterization of multipod, flower-like, and shuttle-like ZnO frameworks in ionic liquids. Materials Letters. 2005, 11, 1405-8.

[15] Kang, X.; Liu, S.; Dai, Z.; He, Y.; Song, X.; Tan, Z. Titanium dioxide: from engineering to applications. Catalysts. 2019, 2, 191.

[16] Whang, T.J.; Hsieh, M.T.; Chen, H.H. Visible-light photocatalytic degradation of methylene blue with laser-induced Ag/ZnO nanoparticles. Applied Surface Science. 2012, 7, 2796-801.

[17] El-Kemary, M.; Abdel-Moneam, Y.; Madkour, M.; El-Mehasseb, I. Enhanced photocatalytic degradation of Safranin-O by heterogeneous nanoparticles for environmental applications. Journal of Luminescence. 2011, 131, 570-6.

[18] Pant, B.; Park, M.; Kim, H.Y.; Park, S.J. Ag-ZnO photocatalyst anchored on carbon nanofibers: Synthesis, characterization, and photocatalytic activities. Synthetic Metals. 2016, 220, 533-7.

[19] Wishart, D.S.; Feunang, Y.D.; Marcu, A.; Guo, A.C.; Liang, K.; Vázquez-Fresno, R.; Sajed, T.; Johnson, D.; Li, C.; Karu, N.; Sayeeda, Z. HMDB 4.0: the human metabolome database for 2018. Nucleic acids research. 2018, 46, (D1):D608-17.

[20] Hasnidawani, J.N.; Azlina, H.N.; Norita, H.; Bonnia, N.N.; Ratim, S. Ali, E.S. Synthesis of ZnO nanostructures using sol-gel method. Procedia Chemistry. 2016, 19, 211-6.

[21] Bekkari, R.; Boyer, D.; Mahiou, R.; Jaber, B. Influence of the sol gel synthesis parameters on the photoluminescence properties of ZnO nanoparticles. Materials Science in Semiconductor Processing. 2017, 71, 181-7.

[22] Mahdavi, R.; Talesh, S.S. The effect of ultrasonic irradiation on the structure, morphology and photocatalytic performance of ZnO nanoparticles by sol-gel method. Ultrasonics Sonochemistry. 2017, 39, 504-10.

[23] Kumaresan, N.; Ramamurthi, K.; Babu, R.R.; Sethuraman, K.; Babu, M. Hydrothermally grown ZnO nanoparticles for effective photocatalytic activity. Applied Surface Science. 2017, 418,138-46.

[24] Ghoderao, K.P.; Jamble, S.N.; Kale, R.B. Influence of pH on hydrothermally derived ZnO nanostructures. Optik. 2018, 156, 758-71.

[25] Bazazi, S.; Arsalani, N.; Khataee, A.; Tabrizi, A.G. Comparison of ball milling-hydrothermal and hydrothermal methods for synthesis of ZnO nanostructures and evaluation of their photocatalytic performance. Journal of industrial and engineering chemistry. 2018, 62, 265-72.

[26] Kumar, S.; Sahare, P.D.; Kumar, S. Optimization of the CVD parameters for ZnO nanorods growth: Its photoluminescence and field emission properties. Materials Research Bulletin. 2018, 105, 237-45.

[27] Narin, P.O.; Kutlu, E.; Atmaca, G.; Atilgan, A.B.; Yildiz, A.; Lisesivdin, S.B. Structural and optical properties of hexagonal ZnO nanostructures grown by ultrasonic spray CVD. Optik. 2018, 168, 86-91.

[28] Jeena, V.; Robinson, R.S. Convenient photooxidation of alcohols using dye sensitised zinc oxide in combination with silver nitrate and TEMPO. Chemical Communications. 2012, 48, 299-301.

[29] Huang, L.; Fan, H. Room-temperature solid state synthesis of ZnO/α-Fe2O3 hierarchical nanostructures and their enhanced gas-sensing properties. Sensors and Actuators B: Chemical. 2012, 171, 1257-63.

[30] Zhang, L. W.; Cheng, H. Y.; Zong, R. L.; Zhu, Y. F. Journal of Physical Chemistry C, 2009, 113, 2368.

[31]. Vasei, H.V.; Masoudpanah, S.M.; Adeli, M.; Aboutalebi, M.R. Solution combustion synthesis of ZnO powders using CTAB as fuel. Ceramics International. 2018, 44, 7741-5.

[32] Ajamein, H.; Haghighi, M.; Alaei, S. Influence of propylene glycol/nitrates ratio on microwave-assisted combustion synthesis of CuO-ZnO-Al2O3 nanocatalyst: Structural and catalytic properties toward hydrogen production from methanol. Materials Research Bulletin. 2018, 102, 142-52.

[33] Anandan, S.; Miyauchi, M. Ce-doped ZnO (Ce x Zn 1− x O) becomes an efficient visible-light-sensitive photocatalyst by co-catalyst (Cu 2+) grafting. Physical Chemistry Chemical Physics. 2011, 33, 14937-45.

[34] Chen, H.; Wen, W.; Wang, Q.; Hanson, J.C.; Muckerman, J.T.; Fujita, E.; Frenkel, A.I.; Rodriguez, J.A. Preparation of (Ga1− x Zn x)(N1− x O x) Photocatalysts from the

Reaction of NH3 with Ga2O3/ZnO and ZnGa2O4: In Situ Time-Resolved XRD and XAFS Studies. The Journal of Physical Chemistry C. 2009, 113, 3650-9.

[35] Patil, A.B.; Patil KRa, AB, and Pardeshi, S.K. Ecofriendly synthesis and solar photocatalytic activity of S-doped ZnO. Journal of Hazardous Materials. 2010, 183, (1-3):315-23.

[36] Chen, L.C.; Tu, Y.J.; Wang, Y.S.; Kan, R.S.; Huang, C.M. Characterization and photoreactivity of N-, S-, and C-doped ZnO under UV and visible light illumination. Journal of Photochemistry and Photobiology A: Chemistry. 2008, 199, 170-8.

[37] Liu, S.; Li, C.; Yu, J.; Xiang, Q. Improved visible-light photocatalytic activity of porous carbon self-doped ZnO nanosheet-assembled flowers. CrystEngComm. 2011, 13, 2533-41.

[38] Shao, D. ; Gao, J. ; Xin, G. ; Wang, Y. ; Li, L. ; Shi, J. ; Sawyer, S. Cl-Doped ZnO Nanowire Arrays on 3D Graphene Foam with Highly Efficient Field Emission and Photocatalytic Properties. *small*, 2015, *11*(36), 4785-4792.

[39] Jiamprasertboon, A. ; Dixon, S. C. ; Sathasivam, S. ; Powell, M. J. ; Lu, Y. ; Siritanon, T. ; Carmalt, C. J. Low-cost one-step fabrication of highly conductive ZnO: Cl transparent thin films with tunable photocatalytic properties via aerosol-assisted chemical vapor deposition. *ACS applied electronic materials*, 2019, *1*(8), 1408-1417.

[40] Peng, X. ; Li, J. ; Liu, X. ; Yi, L. ; Cai, P. ; Wen, Z. Cl-doped carbon nitride nanostrips for remarkably improving visible-light photocatalytic hydrogen production. *International Journal of Hydrogen Energy*, 2021, *46*(56), 28591-28601.

[41] Zhang, P.; Shao, C.; Zhang, Z.; Zhang, M. Mu, J.; Guo, Z.; Liu, Y. TiO2@ carbon core/shell nanofibers: controllable preparation and enhanced visible photocatalytic properties. Nanoscale. 2011, 3, 2943-9.

[42] Zhang, P.; Shao, C.; Zhang, Z.; Zhang, M.; Mu, J.; Guo, Z.; Sun, Y.; Liu, Y. Core/shell nanofibers of TiO 2@ carbon embedded by Ag nanoparticles with enhanced visible photocatalytic activity. Journal of Materials Chemistry. 2011, 21, 7746-53.

[43] Liu, S.; Weng, B.; Tang, Z.R.; Xu, Y.J. Constructing one-dimensional silver nanowire doped reduced graphene oxide integrated with CdS nanowire network hybrid structures toward artificial photosynthesis. Nanoscale. 2015, 7, 861-6.

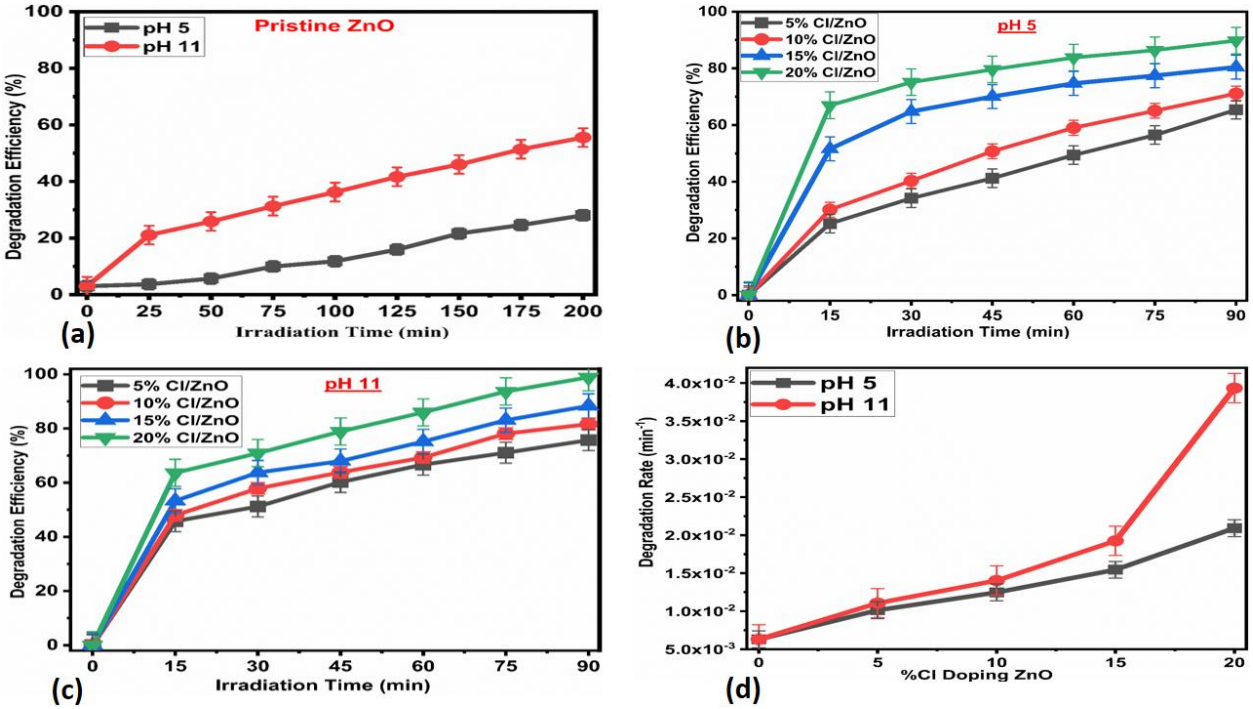

[44] Vignesh, K.; Suganthi, A.; Rajarajan, M.; Sara, S.A. Photocatalytic activity of AgI sensitized ZnO nanoparticles under visible light irradiation. Powder technology. 2012, 224, 331-7.

[45] Gautam, K.; Singh, I.; Bhatnagar, P.K.; Peta, K.R. Role of Cl doping on the growth and relaxation dynamics of ZnO nanorods synthesized by hydrothermal method. Chemical Physics Letters. 2016, 662, 196-200.

[46] Jiamprasertboon, A.; Dixon, S.C.; Sathasivam, S. Powell, M.J.; Lu, Y.; Siritanon, T.; Carmalt, C.J. Low-cost one-step fabrication of highly conductive ZnO: Cl transparent thin films with tunable photocatalytic properties via aerosol-assisted chemical vapor deposition. ACS applied electronic materials. 2019, 1, 1408-17.

[47] Xu, Y.; Zou, J.; Lin, X.; Wu, W.; Li, W.; Yang, B.; Shi, M. Quality-Improved GaN Epitaxial Layers Grown on Striped Patterned Sapphire Substrates Ablated by Femtosecond Laser. Applied Sciences. 2018, 10, 1842.

[48] Nguyen, L.T.; Nguyen, L.T.; Duong, A.T.; Nguyen, B.D.; Quang Hai, N.; Chu, V.H.; Nguyen, T.D.; Bach, L.G. Preparation, characterization and photocatalytic activity of La-doped zinc oxide nanoparticles. Materials. 2019, 8, 1195.

[49] Bhatti, M.A.; Shah, A.A.; Almani, K.F.; Tahira, A. Chalangar, S.E.; dad Chandio, A.; Nur, O.; Willander, M.; Ibupoto, Z.H. Efficient photo catalysts based on silver doped

ZnO nanorods for the photo degradation of methyl orange. Ceramics International. 2019, 45, 23289-97.

[50] Payra, S.; Ganeshan, S.K.; Challagulla, S.; Roy, S. A correlation story of syntheses of ZnO and their influence on photocatalysis. Advanced Powder Technology. 2020, 31,510-20.

[51] Rahman, Q.I.; Ahmad, M.; Misra, S.K.; Lohani, M.B. Hexagonal ZnO nanorods assembled flowers for photocatalytic dye degradation: Growth, structural and optical properties. Superlattices and Microstructures. 2013, 64, 495-506.

[52] Chanu, L.A.; Singh, W.J.; Singh, K.J.; Devi, K.N. Effect of operational parameters on the photocatalytic degradation of Methylene blue dye solution using manganese doped ZnO nanoparticles. Results in Physics. 2019, 12, 1230-7.

[53] Daneshvar, N.; Salari, D.; Niaei, A.; Rasoulifard, M.H.; Khataee, A.R. Immobilization of `TiO2 nanopowder on glass beads for the photocatalytic decolorization of an azo dye CI Direct Red 23. Journal of Environmental Science and Health, Part A. 2005, 40, 1605-17.

[54] lahiane, S.; Qourzal, S.; Ouardi, M.; Abaamrane, A.; Assabbane, A. Am JAnal Chem, 2014, 5, 445.

[55] Tju, H.; Shabrany, H.; Taufik, A.; Saleh, R. Degradation of methylene blue (MB) using ZnO/CeO2/nanographene platelets (NGP) photocatalyst: Effect of various concentration of NGP. InAIP Conference Proceedings. 2017, 1862, 030037. AIP Publishing LLC.

[56] Fox, M.A.; Dulay, M.T. Heterogeneous photocatalysis. Chemical reviews. 1993, 93, 341-57.

[57] Akpan, U.G.; Hameed, B.H. Parameters affecting the photocatalytic degradation of dyes using TiO2-based photocatalysts: a review. Journal of hazardous materials. 2009, 170, (2-3), 520-9.

[58] Sunitha, S.; Rao, A.N.; Abraham, L.S.; Dhayalan, E.; Thirugnanasambandam, R.; Kumar, V.G. Enhanced bactericidal effect of silver nanoparticles synthesized using marine brown macro algae. J Chem Pharma Res. 2015, 7, 191-5.

[59] Kazeminezhad, I.; Sadollahkhani, A. Influence of pH on the photocatalytic activity of ZnO nanoparticles. Journal of Materials Science: Materials in Electronics. 2016, 5, 4206-15.

[60] Dodd, A.C.; McKinley, A.J.; Saunders, M.; Tsuzuki, T. Effect of particle size on the photocatalytic activity of nanoparticulate zinc oxide. Journal of Nanoparticle Research. 2006, 1, 43-51.

[61] Nuengmatcha, P.; Chanthai, S.; Mahachai, R.; Oh, W.C. Sonocatalytic performance of ZnO/graphene/TiO2 nanocomposite for degradation of dye pollutants (methylene blue, texbrite BAC-L, texbrite BBU-L and texbrite NFW-L) under ultrasonic irradiation. Dyes and Pigments. 2016, 134, 487-97.

[62] Rahman, Q.I.; Ahmad, M.; Misra, S.K.; Lohani, M. Efficient degradation of methylene blue dye over highly reactive Cu doped strontium titanate (SrTiO3) nanoparticles photocatalyst under visible light. Journal of nanoscience and nanotechnology. 2012, 9, 7181-6.

[63] Kadhim, M. J. ; Mahdi, M. A. ; Hassan, J. J. Influence of pH on the photocatalytic activity of ZnO nanorods. *Mater. Int.* 2020, 2, 0064-0072.

[64] Bhatti, M. A. ; Almaani, K. F. ; Shah, A. A. ; Tahira, A. ; Chandio, A. D. ; Mugheri, A. Q. ; Ibupoto, Z. H. Low Temperature Aqueous Chemical Growth Method for the Doping of W into ZnO Nanostructures and Their Photocatalytic Role in the Degradration of Methylene Blue. *Journal of Cluster Science*, 2021, 1-12.

[65] Chanu, L. A. ; Singh, W. J. ; Singh, K. J. ; Devi, K. N. Effect of operational parameters on the photocatalytic degradation of Methylene blue dye solution using manganese doped ZnO nanoparticles. *Results in Physics*, 2019, *12*, 1230-1237.

[66]. Sharma, S.; Basu, S. Highly reusable visible light active hierarchical porous WO3/SiO2 monolith in centimeter length scale for enhanced photocatalytic degradation of toxic pollutants. *Separation and Purification Technology*, 2020, *231*, 115916.

[67]. Soltani, N.; Saion, E.; Hussein, M.Z.; Erfani, M.; Abedini, A.; Bahmanrokh, G.; Navasery, M.; Vaziri, P. Visible light-induced degradation of methylene blue in the presence of photocatalytic ZnS and CdS nanoparticles. *International journal of molecular sciences*, 2012, *13*(10), 12242-12258.

[68]. Ebrahimi, A.; Haghighi, M.; Aghamohammadi, S. Sono-precipitation fabrication of ZnO over modified SAPO-34 zeotype for effective degradation of methylene blue pollutant under simulated solar light illumination. *Process Safety and Environmental Protection*, 2022, *165*, 307-322.

[69]. Loke, J.Y.; Zaki, R.M.; Setiabudi, H.D. Photocatalytic degradation of methylene blue using ZnO supported on wood waste-derived activated carbon (ZnO/AC). *Materials Today: Proceedings*, 2022, *57*, 1315-1321.

[70]. Shubha, J.P.; Adil, S.F.; Khan, M.; Hatshan, M.R.; Khan, A. Facile fabrication of a ZnO/Eu2O3/NiO-Based ternary heterostructure nanophotocatalyst and its application for the degradation of methylene blue. *ACS omega*, 2021, *6*(5), 3866-3874.